Marine Pollution Bulletin 135 (2018) 1145–1157

Contents lists available at ScienceDirect

Marine Pollution Bulletin

journal homepage: www.elsevier.com/locate/marpolbul

Proof of concept for a model of light reflectance of plastics floating on natural waters

Lonneke Goddijn-Murphy*, Juvenal Dufaur

Environmental Research Institute, UHI-NHC, Thurso, Scotland, UK

ARTICLE INFO

Keywords:
Plastic debris
Remote sensing
Marine environment
Natural waters
Pollution

ABSTRACT

Remote sensing of plastic littering natural waters is an emerging field of science with the potential to provide observations on local to global scales. We present the verification of a theoretical reflectance model of sunlight interacting with a water surface littered with buoyant plastic objects. We measured a few common litter items of different polymers as well as shapes, transparencies, and surface roughnesses. Spectral reflectance measurements in the field were backed up with measurements in the laboratory of coefficients of total and diffuse reflectance, transmittance and absorption. We evaluated a single-band algorithm for 850 nm wavelength and a dual-band algorithm using a second wavelength at a polymer absorption band between 1660 and 1730 nm. Both algorithms were plastic litter type specific. Our findings show that for interpreting spectral remote sensing of floating plastic, physical properties that control geometrical optics should complement information about the absorption spectra of the polymer.

1. Introduction

1.1. Background

Remote sensing (RS) of plastic pollution of natural waters is still in its early stages despite increasing concern about the environmental impacts and the lack of long-term, large scale monitoring. Each year an estimated 4.8 to 12.7 million metric tons (MT) of plastic enters the oceans from land and without waste management, plastic litter entering the ocean is predicted to increase by an order of magnitude by 2025 (Jambeck et al., 2015). Schmidt et al. (2017) estimate the global plastic debris inputs from rivers into the sea alone to range between 0.41 and 4 MT per year. Plastic persists in the environment for very long times (centuries); it can be lost from the sea by sinking to the bottom, beaching, degradation, and ingestion by animals. While ultraviolet light of the sun and chemicals dissolved in seawater degrade the plastic, breaking waves and collisions fragment macroplastics (> 5 mm) into smaller and smaller pieces and finally into microplastics (< 5 mm). Exactly what happens to marine plastic litter is uncertain as global budgeting exercises find significantly less material on the ocean surface than expected (Cózar et al., 2014; Eriksen et al., 2014; van Sebille et al., 2015). Some surveys of sea surface plastic debris have been undertaken in the global oceans (e.g., Law et al., 2010, 2014; Cózar et al., 2014, 2017; Eriksen et al., 2014; Lebreton et al., 2018) but there are still large data gaps. Three largely independent ocean circulation models have produced global microplastic distribution maps (Lebreton et al., 2012; Maximenko et al., 2012; van Sebille et al., 2012). The models agree reasonably well within the centres of the gyres where plastic debris accumulates and concentrations are high, but they strongly differ in the tropics, the high latitudes, and the Eastern Mediterranean (van Sebille et al., 2015). In the gyre centres, the weight density of plastic pollution is dominated by the largest size class (> 200 mm) and estimated to be in the order of 10,000 g km^{-2} (Eriksen et al., 2014). Lebreton et al. (2018) recently reported exponentially increasing levels of ocean plastic pollution in the Great Pacific Garbage Patch (GPGP). Here they estimated at least 79 (45–129) thousand tonnes of ocean plastic floating inside an area of 1.6 million km^2 (three to eight times higher than 10,000 g km^{-2}) with over three-quarters of its mass consisting of debris larger than 5 cm. Lebreton et al. (2018) conducted aerial imagery using an aircraft mounted RGB camera to improve recordings of larger debris (> 0.5 m) and increase the size of their survey area (311 km^2). The images were inspected by trained human observers and an experimental image processing algorithm capable of detecting potential debris applied to all their RGB imagery.

Remote sensing observations to verify the ocean circulation models of plastic particles have not yet been made. Maximenko et al. (2016) describe how remote sensing could answer basic questions about the dynamics of plastic debris that have so far remained unanswered. They

* Corresponding author at: Environmental Research Institute, CfEE Building, UHI-NHC, Ormlie Road, Thurso KW14 7EE, Scotland, UK.
E-mail address: Lonneke.Goddijn-Murphy@uhi.ac.uk (L. Goddijn-Murphy).

https://doi.org/10.1016/j.marpolbul.2018.08.044
Received 30 July 2018; Received in revised form 20 August 2018; Accepted 20 August 2018
Available online 01 September 2018

propose different promising RS technologies (optical observations, imaging spectroscopy, Synthetic Aperture Radar (SAR), and Raman spectroscopy), not just for satellite sensors but also for airborne-, shipborne-, onshore-, and handheld sensors. We studied hyperspectral RS for buoyant macroplastics in the visible (VIS) to near infrared (NIR) to short wave infrared (SWIR) spectrum, comprising wavelengths from 350 to 1790 nm. In this paper we present the experimental results by validating our theoretical reflectance model of sunlight interacting with a water surface littered with macroplastics and evaluate RS algorithms based on this model (Goddijn-Murphy et al., 2018). We were particularly interested in how physical properties of the plastic items affected light reflectance and the performance of our model, and selected a few items accordingly. As this was a proof of concept experiment, we felt this to be acceptable. The theoretical model and RS algorithms are not exclusively applicable to the ocean but also to inland waters where plastic littering is a problem (e.g., Driedger et al., 2015; Hoffman and Hittinger, 2017).

Objects larger than a couple of radiance wavelengths (in the order of micrometres in the VIS-SWIR spectrum) can reflect this radiance (Hecht and Zajac, 1974), thus microplastics would in theory be included in our optical model. However, wind driven ocean mixing removes buoyant microplastics from the top of the ocean surface (Kukulka et al., 2012; Kooi et al., 2016). We therefore do not expect our method to be successful for the detection of microplastics, but by studying macroplastics we study a major and increasing source of microplastics (Filella, 2015). The optical signal of microplastics particles suspended in the water body would be better explained by their absorption (a) and backscattering (b_b) coefficients in analogy to those of suspended sediments and phytoplankton (Gordon et al., 1975; Morel and Prieur, 1977). However, well over 50% of marine microplastics are found below the top 15 cm of the ocean surface (Kooi et al., 2016) where most light in the NIR and SWIR is absorbed by water (Irvine and Pollack, 1968). Biofouling will reduce the buoyancy of plastic particles, so that they sink below the sea surface and the smaller their size, the sooner they sink due to the higher surface area to volume ratio (Ryan, 2015).

Although hyperspectral RS for the detection of marine litter has been suggested before (e.g., Veenstra and Churnside, 2012; Driedger et al., 2015; Maximenko et al., 2016), until recently few reflectance spectra of marine plastic litter were published. Goddijn-Murphy et al. (2018) used spectra of plastic bottles presented by Asner (2016) to support their theoretical concept model of hyperspectral reflectance. Since then, Garaba and Dierssen (2018) published daylight reflectance spectra of marine-harvested micro- and macroplastics and 'virgin' microplastic pellets for the 350–2500 nm wavelength range. The microplastics were aggregated into an optically dense target on a low reflectance black rubber mat and the reflectance of wet marine-harvested microplastics was also measured. We used the same spectroradiometer to measure daylight reflectance of buoyant macroplastics floating on top of water. Our approach was to evaluate how transparency, optical surface roughness, shape and size changed reflectance. We show that these optical properties of the plastic litter items should complement reflectance measurements of plastics in the form of aggregated pellets (Garaba and Dierssen, 2017, 2018) and of one layer of plastic in air (Fig. 4). The lighting environment during our outdoors measurements were far from optimal, but we could still use our results to help understand the interaction of sunlight with floating plastic items. In addition, we measured spectra of coefficients of total and diffuse reflectance, transmittance and absorption in the laboratory (Fig. 4), using the spectroradiometer as a desktop instrument with its own light source.

1.2. Concept model

Goddijn-Murphy et al. (2018) developed a model to explain light reflectance of buoyant plastic floating on waters, based on geometrical optics and the spectral signatures of plastic and water. They include all reflectance- and transmittance contributions of upwelling and downwelling light and then take out the smallest terms. Goddijn-Murphy et al. (2018) define reflectance R as L/E_d [sr^{-1}], with L [$Wm^{-2}sr^{-1}$] upwelling radiance in nadir view and E_d [Wm^{-2}] downwelling irradiance. In this current paper, we redefine R as dimensionless L/L_d with L_d the radiance reflected off a Lambertian reflectance panel (Lambertian reflected light is scattered equally in all directions so that $L_d = E_d/\pi$). This definition of reflectance compared more directly with our measurements which were made using the spectroradiometer in "white reference mode" and a Lambertian reference panel. In the present paper we consequently use definitions of total reflectance $R_t = L_t/L_d$ (with L_t total water and plastic leaving radiance), water reflectance in the absence of plastic $R_{w,0} = L_{w,0}/L_d$, and plastic reflectance $\rho_p = L_{pr}/L_d$ (with L_{pr} light reflected at plastic in air). Water leaving radiance, $L_{w,0}$, is the sum of light that is reflected directly at the air-water interface and light that is transmitted from below. For low subsurface water reflectance, subsurface upwelling light transmitted upwards through the plastic is neglected and reflectance at wavelength, λ, can be estimated using

$$R_t(\lambda) = \varepsilon(f,\lambda)R_{w,0}(\lambda) + f\left(\rho_p(\lambda) - \varepsilon(f,\lambda)R_{w,0}(\lambda)\right) \quad (1)$$

(Goddijn-Murphy et al., 2018). In Eq. (1), f is fraction of surface plastic and ε is defined as "shading factor", a factor to account for the reduction of underwater light due to plastic floating on top of it. This factor is expected to be close to one, especially for small f. If ρ_p is known and we can estimate $R_{w,0}$, we can calculate f as $(R_t - R_{w,0}) / (\rho_p - R_{w,0})$ (Eq. (1)) for an area in nadir view, using ρ_p at a wavelength where reflectance is high. But if we do not know $R_{w,0}$ a priori, we could apply more than one wavelength to derive f. For example, if we can find a second wavelength, λ_2, for which $R_w(\lambda_1) \approx R_w(\lambda_2)$ while $\rho_p(\lambda_1) \neq \rho_p(\lambda_2)$ then,

$$f(\lambda_1,\lambda_2) = \frac{R_t(\lambda_1) - R_t(\lambda_2)}{\rho_p(\lambda_1) - \rho_p(\lambda_2)} = \frac{R_t(\lambda_1) - R_t(\lambda_2)}{\Delta\rho_p(\lambda_1,\lambda_2)} \quad (2)$$

(Goddijn-Murphy et al., 2018).

Natural downwelling light is a combination of direct light (the solar beam) and diffuse light (skylight). The ratio diffuse/total (F) depends on sky conditions (e.g., clouds and haziness) and increases with decreasing solar altitude and decreasing wavelength (Jerlov, 1968). Similarly, radiance reflectance at a surface can be specular (Fresnel reflection) and diffuse (in all directions), the former occurs at an optically smooth- and the latter at an optically rough surface. If we consider reflectance at an optically smooth surface, light received in nadir view consists of specular reflected skylight as the sun is generally not in zenith. At an optically rough surface, diffuse reflectance of the solar beam also contributes to nadir reflected light. Both the water surface and the plastic litter can have specular and diffuse reflecting properties. Goddijn-Murphy et al. (2018) apply their model to Fresnel reflectance of diffuse skylight. In this study, we found in the laboratory that the diffuse reflectance coefficient, r_{dif}, dominated the total reflectance coefficient, r, so that diffuse reflectance of all light (skylight + solar beam) should have been included in their model. An aim of this study was to find if we could use r_{dif} and r to predict ρ_p for plastic floating on water. RS of water quality is traditionally done at high solar angles and under clear skies. Under these conditions, direct reflectance at the water surface is minimized so that the proportion of water leaving light from below the surface, the light that contains information about the water body, is maximized. In our RS method for floating plastic litter we use the reflecting properties of the water and plastic surface and the more different those are, the more successful it should be. The lighting conditions may therefore be less critical and sufficient for testing the model.

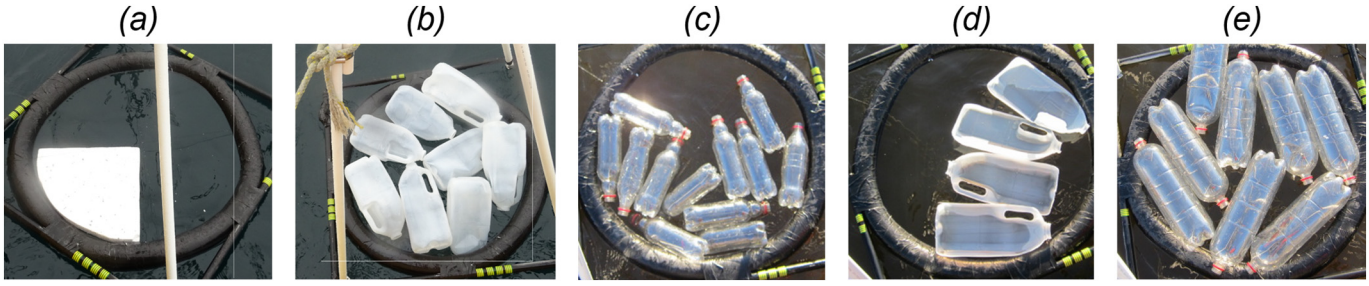

Fig. 1. (a) EPS, building foam, $f' = 0.25$, (b) HDPE whole milk bottles, $f' = 1$, (c) PET, 0.5 L bottles, $f' = 0.75$, (d) HDPE, half milk bottles, $f' = 0.5$, and (e) PET, 2 L bottles $f' = 1$.

2. Methodology

2.1. Plastic objects

We measured light reflectance of a number of buoyant plastic litter items generally littering the ocean. Eriksen et al. (2014) most frequently observed polystyrene foam, also known as expanded polystyrene (EPS), in marine plastic litter. They report that from 891 visual survey transects in the global oceans (across all five sub-tropical gyres, coastal Australia, Bay of Bengal and the Mediterranean Sea), 1116 out of 4291 macroplastic items are composed of EPS. In contrast, Lebreton et al. (2018) found a minimal contribution of foamed plastic items in GPGP, reminding us how the constituents of marine plastic litter can vary from one place to another. In our experiment we used a 2.3 cm thick sheet of white, grey speckled EPS, cut into quadrants of 28 cm radius (Fig. 1a). The next most counted macroplastic item by Eriksen et al. (2014), other than miscellaneous, is the plastic bottle with 791 items. We measured white, semi-transparent, 2 L milk bottles made of high-density polyethylene, HDPE, (Fig. 1b) and clear, transparent soft drink bottles made of polyethylene terephthalate, PET, (Fig. 1c & e). Downwelling sunlight passing through a floating bottle is transmitted through, and reflected by, two layers of plastic of which the top one is in air. We cut milk bottles along their lengths (Fig. 1d) and measured light reflectance of a single layer floating on the water surface to assess the difference. A bottle's size should modify its optical geometry and we compared small (0.5 L) PET bottles (Fig. 1c) and large (2 L) PET bottles (Fig. 1e). The plastic item's reflectance height dependence was also assessed by stacking up to six EPS quadrants on top of each other. The details of the macroplastic items studied in this paper are summarized in Table 1. The plastic items were clean and free from biofouling, in their original shape, and contained no water or other liquid. It was difficult to control the wetness of our litter items during the experiments in the field and we considered their surfaces to be a mix of wet and dry. During the measurements in the laboratory, the plastics were dry.

Of a surface area, A_t, we considered plastic surface area, A_p', as the surface area on which the plastic objects floated without overlap but including small gaps in, and between, object shapes (Fig. 1). We defined f' as A_p'/A_t, a parameter equal or approximate to f; because f' is proportional to f, we could use f' to verify Eqs. (1) and (2). Ideally, we would have a large area covered with floating plastic items and take reflectance measurements in the centre, far enough away from the area's edge to exclude the contributions of open water leaving light. In our experiment, the ground field of view (FOV) was the 20 cm radius disk centred in a floating ring (Fig. 2). The ring's enclosure was divided in four quadrants by thin black iron yarns to facilitate a partition. By filling one, two, three and all four quadrants we derived corresponding values for fractional plastic surface area, f', of {0.25, 0.5, 075, 1} for the area within the ring and all smaller concentric circular areas within.

2.2. Spectroradiometer in the field

Hyperspectral light reflectance measurements were carried out with the Analytical Spectral Devices (ASD) FieldSpec Pro, a field spectroradiometer with a spectral range from 350 to 2500 nm and data interpolated to 1 nm wavelength steps. We used the instrument in white reference mode with a calibrated white Spectralon® reflectance panel. The instrument's light sensor, with a fore optics field of view (FOV) of 18° attached, was mounted on the floating frame at 126 cm nadir height above the water surface and connected to the spectroradiometer with a 1.4 m fiber optic light guide (Fig. 2). Thus, a circular area of 20 cm radius was in view, centred in the 28 cm radius area enclosed by the matte black, floating ring. We measured reflectance values of the open water surface ($R_{w,0}$) and R_t for plastic surface fractions $f' = \{0.25, 0.5, 0.75, 1\}$.

The responsivity of the ASD FieldSpec Pro can be uneven across the measurement field (Mac Arthur et al., 2012). Also, the positioning of the plastic items in the ring could be affecting R_t. For each f' value we therefore took four repeat measurements by filling different quadrants with plastic, averaging the four measurements and calculating the standard error of the mean (SE). ($f' = 0.25$ was measured by filling quadrant 1, 2, 3 or 4; $f' = 0.5$ by filling quadrants 1-2, 2-3, 3-4, or 4-1; $f' = 0.75$ by filling quadrants 1-2-3, 2-3-4, 3-4-1, or 4-1-2.) Following

Table 1
The different plastic litter types used in the experiment. N is number of items that fit in one quadrant of the area under consideration (Fig. 1); V is volume, l is length, w is width, h is height, and m is weight of one item; 'Name' indicates how object is referred to in this text.

Item	Polymer	N	V (l)	l (cm)	w (cm)	h (cm)	m (g)	Surface	Optical properties	Name Fig.
Insulation sheet	Expanded polystyrene	1	1.4	28 radius		2.3	29	Flat	Opaque white, grey specks	EPS 1a
Milk bottle	High-density polyethylene	2	2	25	12	9	32	Flat/convex	Semi-transparent white	HDPE 1b
Milk bottle cut in half	High-density polyethylene	2	na	25	12	4.5	16	Flat/concave	Semi-transparent white	HDPE_h 1d
Soft drink bottle small	Polyethylene terephthalate	4	0.5	22.5	6 diameter		20	Cylindrical	Transparent clear	PET 1c
Soft drink bottle large	Polyethylene terephthalate	2	2	33	10 diameter		42	Cylindrical	Transparent clear	PET_L 1e

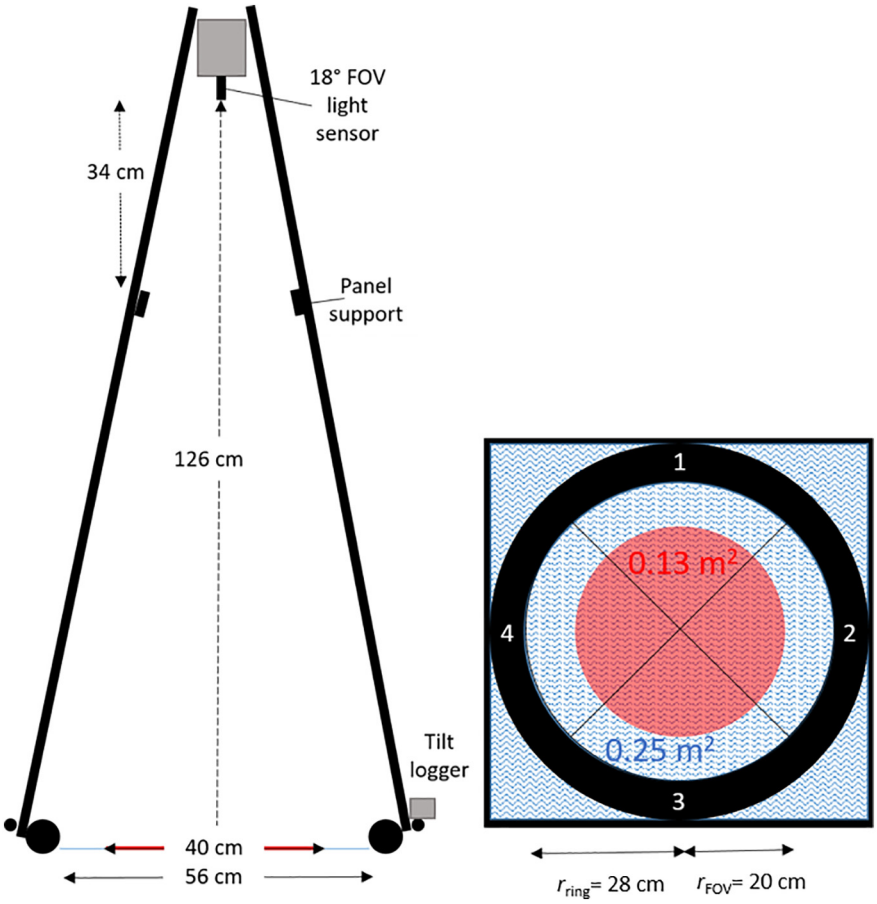

Fig. 2. Experimental set up of the field experiment showing the floating frame viewed from, (left) the side with the light sensor in the top and the diameter FOV on the ground in red, and (right) above with ground FOV in red. The frame was constructed using white pvc pipes in a pyramid shape and held afloat by a matte black buoyant ring, divided in four quadrants by black iron yarn. Total ground FOV was 0.13 m^2 and total area under consideration within the ring, A_t, was 0.25 m^2. Panel support was fixed 34 cm below the sensor to keep the Spectralon® reflectance panel in place during optimization and white reference measurements.

Garaba and Dierssen (2018), we smoothed the measured spectra using a moving average filter with a span of 19 nm, before calculating their mean. Before each measurement series of a plastics item ($f' = 0$ to 1), and also when the lighting conditions noticeably changed, we optimized the FieldSpec Pro and took a white reference measurement. For this we placed the calibrated Spectralon® panel 34 cm below the sensor. In the field, one FieldSpec Pro reflectance data record was an average of 30 samples with a sample time of 68 ms or 136 ms depending on light levels, resulting in a scan time of 2 s or 4 s. Due to low light levels during our measurements, the data was generally noisy beyond the second water absorption band and we decided to only use our measurements at smaller wavelengths (< 1790 nm). We also removed all data from the water absorption band, 1350 nm–1460 nm. A HOBO UA-004-64 Pendant G logger was mounted on the bottom of the frame (Fig. 1) for 1 Hz measurements of the pitch and roll of the frame during the light reflectance recordings. We used the tilt angels as a measure of water surface roughness, which could affect water surface reflectance as well as reflectance of the objects floating on it.

2.3. Spectroradiometer in the laboratory

In addition to fieldwork, we measured spectral coefficients of diffuse reflectance (r_{dif}), total reflectance (r), transmittance (t), and absorption (a) of the plastic using the ASD FieldSpec Pro as a desktop spectroradiometer with ASD accessories that contain their own light sources. The experiment took place with the window blinds down and the lights off but not in complete darkness. The instrument was used in white reference mode with an integration time of 136 ms and 100 samples per data value and we applied a moving average filter with a 19 nm span to the spectra. For deriving r_{dif}, we attached ASD's high intensity contact reflectance probe and measured light reflected from one layer of plastic pressed on top of a black light absorbing panel. For estimating r and t, we used an ASD reflectance/transmittance integrating sphere with the light source setting on 'high' to measure one layer of plastic. We applied ASD's recommended method which corrects for substitution error, whereby the white reference was run with the integrating sphere in the reference configuration (ASD Inc., 2008). The total reflectance coefficient is the sum of diffuse reflectance, r_{dif}, and specular reflectance, r_{spe},

$$r(\lambda) = r_{spe}(\lambda) + r_{dif}(\lambda) \tag{3}$$

The coefficient of absorption, a, can be derived from r and t as their sum equals one,

$$r(\lambda) + t(\lambda) + a(\lambda) = 1 \tag{4}$$

Light hitting a (semi) transparent plastic bottle is reflected by, and transmitted through, two layers of plastic. Nadir plastic leaving light reflected by two parallel sheets of plastic in air can be described as the sum of reflectance from top and from bottom layer (Fig. 3), so that $L_p = (r + t^2r + t^2r^3 + t^2r^5 + \ldots)L_d = r(1 + t^2(1 + r^2 + r^4 + \ldots))L_d$. Using the Taylor expansion for $1/(1 - x)$, reflectance for the two layers, r_2, can be described by,

$$r_2(\lambda) = r(\lambda)\left(1 + \frac{t(\lambda)^2}{1 - r(\lambda)^2}\right) \tag{5}$$

According to Eq. (5), reflectance of two separated layers of plastic in air would be $[1 + t^2/(1 - r^2)]$ times higher than that of one single layer.

Naturally, measuring plastic reflectance in the laboratory was different from measuring plastic reflectance in the field where the plastic item is floating on top of the water surface so that its underside is in contact with water and not with air. Water has a higher refractive index ($n = 1.33$) than air ($n = 1.00$) and is closer to that of plastic ($n = 1.54$

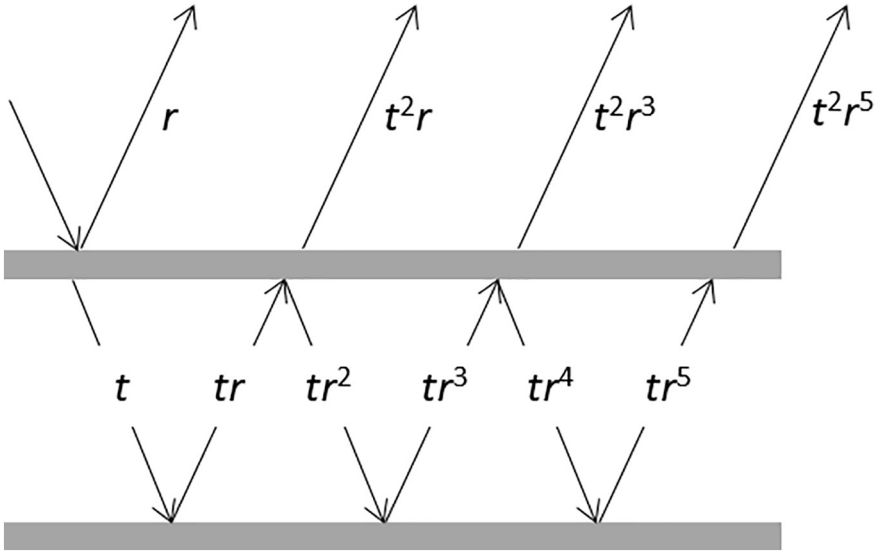

Fig. 3. Diagram showing reflectance of light passing through two separated layers of (semi) transparent plastic in air.

for HDPE and $n = 1.575$ for PET (Scientific Polymer and Inc, 2013)). Reflectance of light at the plastic-water interface will therefore be smaller than at the plastic-air interface (Hecht and Zajac, 1974). This can be clearly recognized in Fig. 1d where the plastic in contact with water is visibly darker. In conclusion, the reflectance of a (semi-) transparent layer of plastic floating on top of the water surface was therefore expected to be lower than r, and of a plastic bottle higher than r but lower than r_2.

2.4. Survey conditions

We did three surveys between 10 and 18 October 2017 in a boating pond in Thurso, Scotland (58°35′27″N, 3°31′15″W) at a latitude where we only had a two to four hour time window when solar elevation angles were higher than ~20°. Although the present lighting conditions (Table 2) were not those that usually support airborne or satellite remote sensing (clear skies, high solar elevation angles), our measurements did reveal characteristics of light interacting with floating plastic items. At 20° solar elevation and for a clear sky, the percentage of skylight is about 80% for 397 nm and 13% for 764 nm (Jerlov, 1968), and this percentage was expected to have been higher during our surveys due to the presence of clouds in the sky.

The water in the boating pond is connected to Thurso River, a small river that drains a peat-rich catchment and is full of humic substances (Batchelli et al., 2010). The pond contains these humic substances too but is likely more complex with additional suspended minerals and algal products. The water in the pond looked very dark. We measured from the side of the pond where both the water depth and Secchi disk depth were 0.9 m. Surface roughness estimated by tilt angle of the frame was highest during survey 2, but overall very small (Table 2).

Table 2
Survey details. Tilt angle is minimum to maximum average pitch or roll angle of the frame during a FieldSpec Pro recording (average over a measurement series of a plastic item).

Survey	Date	Time (GMT)	Solar elevation	Sky[a]	± tilt angle
1	10 Oct 2017	1104–1210	23.5°–24.6°	5	0.9°–1.3°
2	12 Oct 2017	1027–1220	21.4°–23.6°	2, 3, 7	1.3°–4.4°
3	18 Oct 2017	1140–1309	21.2°–21.6°	6, 7	0.6°–1.2°

[a] Sky code as in the NERC FSF Data Log. [2] Thin Cirrus - sun not obscured; [3] Thin Cirrus - sun obscured; [5] Cumulus over most of the sky - sun not obscured; [6] Cumulus - sun obscured; [7] Complete cumulus cover.

3. Results

3.1. Reflectance spectra

Our reflectance, transmittance and absorption spectra measured using the contact probe and integrating sphere are plotted in Fig. 4. The reflectance spectra r and r_{dif} are replicated in Fig. 5 where our field measurements are plotted. In Fig. 5 blue shows open water reflectance, and the shades of grey reflectance with a range of plastic fractions added. We found that the signal-to-noise ratio of the spectral reflectance measurements decreased with increasing wavelength and with decreasing light intensity.

3.1.1. Water reflectance

Open water reflectance, $R_{w,0}$, did not reveal distinguished spectral features. For surveys 1 and 2, water reflectance decreased with increasing wavelength and was under 1% for wavelengths over 400 nm and towards 0.5% near 1800 nm. For survey 3, the reflectance was higher, being 2.5% and 1.5% respectively. Blue light absorption, as is typical for humic substances (e.g., Bowers et al., 2000), was not recognized in the spectra as reflectance did not weaken towards the shorter end of the spectrum. This could be because of enhanced backscattering towards the lower end of spectrum by colloid material (Stramski and Woźniak, 2005). For survey 3, the higher reflectance was believed to be reflectance enhanced by a larger proportion of diffuse skylight due to the lighting conditions (Table 2).

3.1.2. EPS, building foam

Laboratory. The sheet of EPS building foam was the most effective reflector with r of roughly 90% and an absorption peak at around 1680 nm ($r = 67\%$) and a smaller one ($r = 85\%$) around 1140 nm (Fig. 4a). Diffuse and total reflectance were practically similar, indicating that for EPS specular reflectance was near zero (Eq. (3)); no light was transmitted through the sheet (Fig. 4a).

Field. The measured field spectra, R_t, for different levels of f' are illustrated in Fig. 5a–c, together with $R_{w,0}$, r, and r_{dif}. During the first field survey, R_t for full EPS coverage agreed well with the spectra derived in the laboratory. For decreasing f', R_t dropped accordingly over the whole width of the spectrum, with the EPS absorption peaks becoming shallower. During the consequent surveys, R_t was lower for f' of 1 and 0.75 but not for smaller f'. During survey 3, R_t dropped steeply either side of the water absorption band.

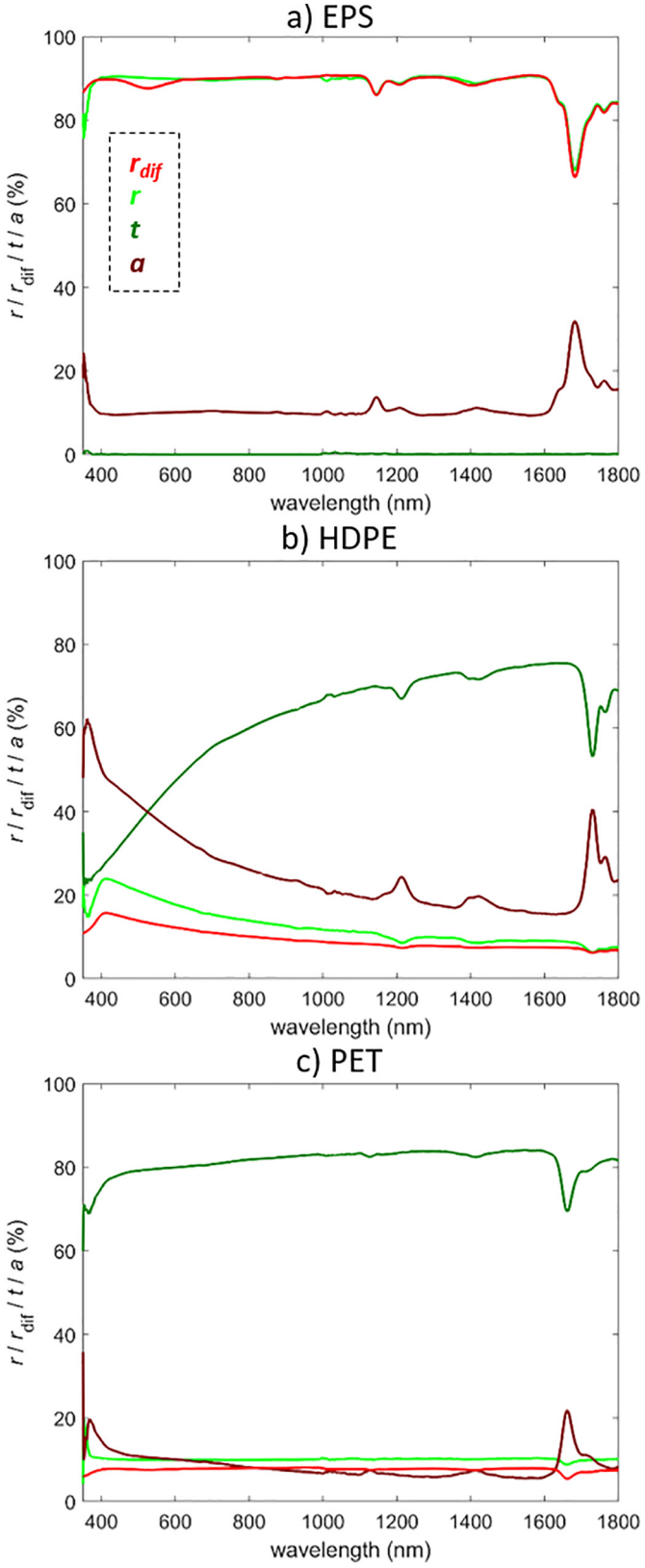

Fig. 4. Line plots showing total and diffuse reflectance coefficients, r and r_{dif}, and transmittance coefficient, t, of one layer of plastic in air measured in the laboratory, and absorption coefficient, a, derived from r and t (Eq. (4)). For (a) EPS foam building sheet, (b) HDPE milk bottle, and (c) PET drink bottle; with r/r_{dif} in light green/red, and a and t in dark red and green respectively. (For interpretation of the references to colour in this figure legend, the reader is referred to the web version of this article.)

3.1.3. HDPE, milk bottles

Laboratory. The overall reflectance of HDPE milk bottle plastic was lower than of EPS (Fig. 4b); this was expected seeing that the plastic was semi-transparent. For one layer of plastic, r peaked at 24% at 410 nm, dropping off at lower and higher wavelengths and with absorption bands around 1210 nm and 1730 nm. Specular reflectance was significant, regarding the specular (diffuse) reflectance coefficient was 8% (16%) at its peak. The proportion of diffuse reflectance increased with increasing wavelength, from about $r_{dif} = 0.65r$ at 410 nm to $r_{dif} = 0.92r$ at 1790 nm.

Field. During the first survey, peak R_t at 429 nm (the centre of the band somewhat shifted to the right compared to r) was 39.4% for $f' = 1$, over 1.5 times higher than r (Fig. 5d) and significantly higher than 1.1 times as calculated using Eq. (5) with $t = 30\%$. (This was further investigated using halved, single-layer milk bottles, which will be discussed later.) During the first and third survey, R_t followed r most closely for f' of 0.5 while during the second pond survey, R_t was at a lower level and followed r more closely for f' of 0.75 (Fig. 5e). For all surveys, overall reflectance increased with increasing f' while the absorption bands deepened, exposing the absorption bands around 1210 nm and 1730 nm clearly. Between the water absorption band and the right end of the spectrum, R_t was raised around 1600 nm, a feature best pronounced in the first survey but not recognized in the laboratory spectra (Fig. 4b). We have no clarification for this bump in R_t.

3.1.4. PET, small drink bottles

Laboratory. The clear PET soft drink bottles were the least effective reflectors (Fig. 4c). Reflectance of a layer of the PET was fairly wavelength independent, with r (r_{dif}) fluctuating around 10% (just below 8%) between 400 nm and 1790 nm, except for a distinctive absorption band around 1660 nm. We found a slighter absorption band in the water absorption band at 1410 nm.

Field. The spectra of R_t obtained in the field showed a combination of $R_{w,0}$ and r (Fig. 5g–h). R_t decreased with increasing wavelength, signifying the spectral shape of $R_{w,0}$ (seeing r was near constant). During both surveys, R_t was closest to r_{dif} and well under r for high f'. Evidence of the 'two layers effect' was therefore absent. The PET absorption band at 1660 nm was distinguished in R_t and deepened with increasing f'.

3.2. The effects of item shape and size

Plastic litter is generally not in the shape of a flat, single layered sheet (or two parallel sheets) as described by the model, and during survey 3, the effects of shape and size of the different items on their spectral reflectance properties were investigated.

3.2.1. EPS, height

Quadrants of EPS (Fig. 1a) were stacked on top of each other to investigate the effect of item height on R_t for f' of 0.25. The spectra (Fig. 6) show how R_t increased with increasing height from 2.3 cm (one layer) to 13.8 cm (six layers), demonstrating that the sides also contributed to light received in nadir view. This included light reflected via the surrounding water surface, as we could see a reflection of the stack's sides on the water surface. The rate of increase was wavelength dependent and stronger for wavelengths beyond the water absorption band. For shorter wavelengths ($\lambda < 1350$ nm), the R_t rate of increase with stack height appeared to level off.

3.2.2. HDPE, halve, single-layer plastic milk bottles

Milk bottles cut along their lengths (Fig. 1d) were used to evaluate the reflectance of one single layer in the water. R_t spectra for the range of f' values (Fig. 7a) show that for the single-layer plastic items, R_t was significantly lower than for the whole, double-layer bottles (Fig. 5f).

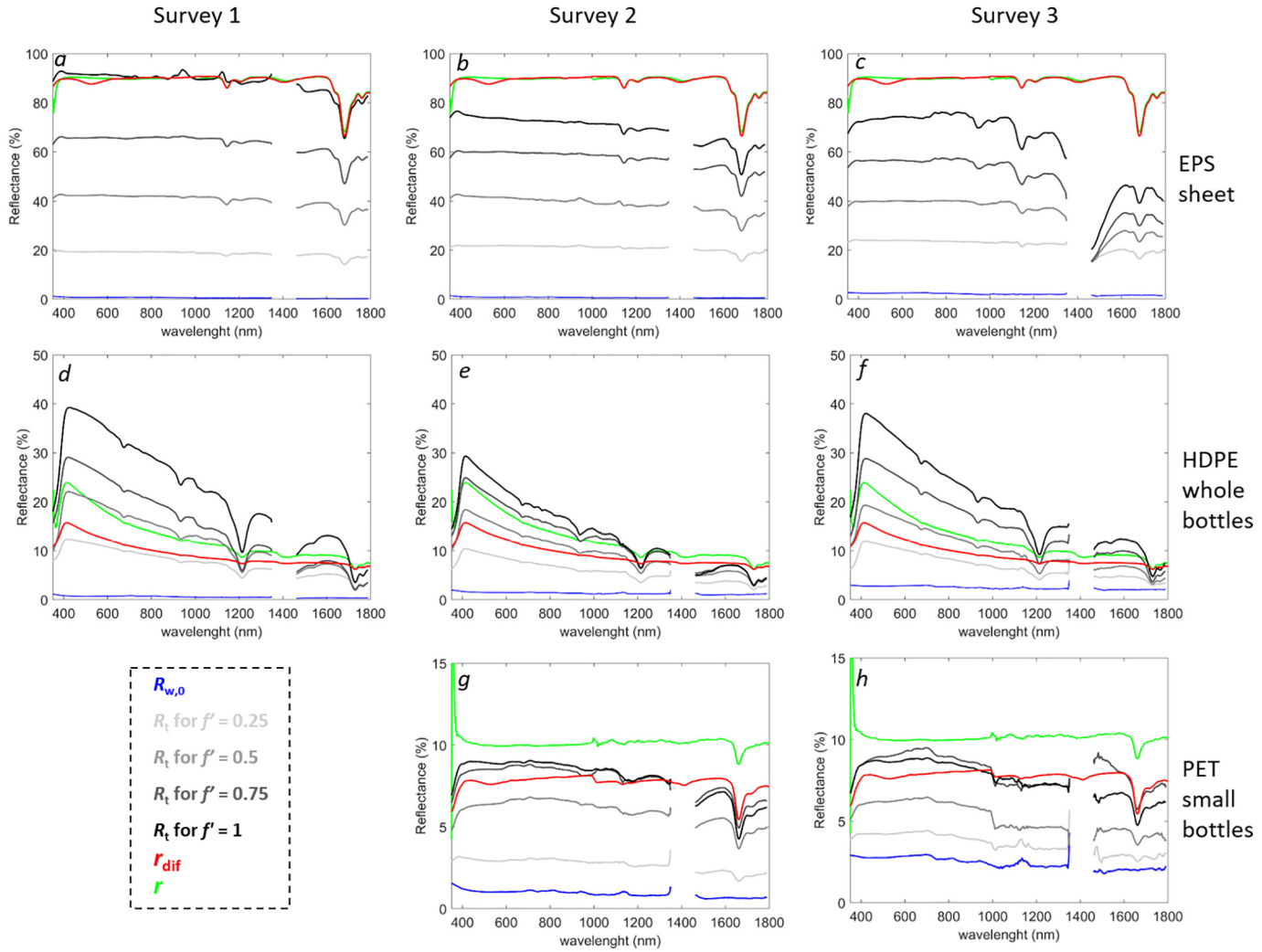

Fig. 5. Line plots of reflectance measurements of in situ plastic with from left to right, surveys 1, 2, and 3, and from top to bottom EPS foam sheet, HDPE milk bottle and PET small bottle. Grey indicates R_t for $f' = \{0.25, 0.5, 0.75, 1\}$ and blue indicates $R_{w,0}$. Green and red respectively indicate r and r_{dif} of one layer of plastic in air measured in the laboratory (Fig. 4). (For interpretation of the references to colour in this figure legend, the reader is referred to the web version of this article.)

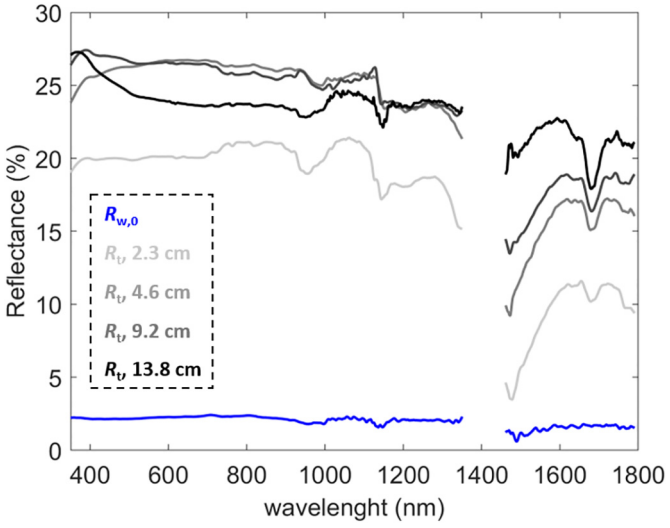

Fig. 6. Line plots of R_t of one quadrant of EPS building foam ($f' = 0.25$), floating in the pond for a range of heights (2.3, 4.6, 9.2, and 13.8 cm) indicated in shades of grey; $R_{w,0}$ is plotted in blue. (For interpretation of the references to colour in this figure legend, the reader is referred to the web version of this article.)

Over the whole spectrum, R_t was lower than r, and for $\lambda < 1350$ nm and $f' = 1$ close to r_{dif}. This could be explained by the underside of the plastic being in contact with water instead of air, reducing light reflectance. The single layer HDPE appeared visibly darker where it came in direct contact with the water it was floating on (Fig. 1d). The ratio of R_t for uncut milk bottles divided by R_t for half milk bottles varied between about 1.5 and 2.5 (Fig. 7b). The corresponding ratio (r_2/r) estimated using Eq. (5) increased from about 1.1 to 1.5 with increasing wavelength up to the HDPE absorption band at 1730 nm. Eq. (5) therefore noticeably underestimated consequences of halving the bottle. We can think of a couple of causes for this underestimation. Firstly, Eq. (5) does not take into account reduced reflectance of the bottom layer due to it being in contact with water instead of air. Secondly, item height can significantly enhance light reflectance in nadir view, as we saw for the EPS foam sheets. Also, the halved milk bottles were on the water with the concave side facing up which was likely to reflect light differently than the convex side of the whole bottle.

3.2.3. PET, large drink bottles

In addition to using small PET drink bottles (Fig. 1c), large PET bottles (Fig. 1e) were used during survey 3 to measure spectral reflectance. R_t for large bottles mostly varied around r for f' of 0.75 (Fig. 8a) while for the small bottles R_t was smaller than r for f' of 1

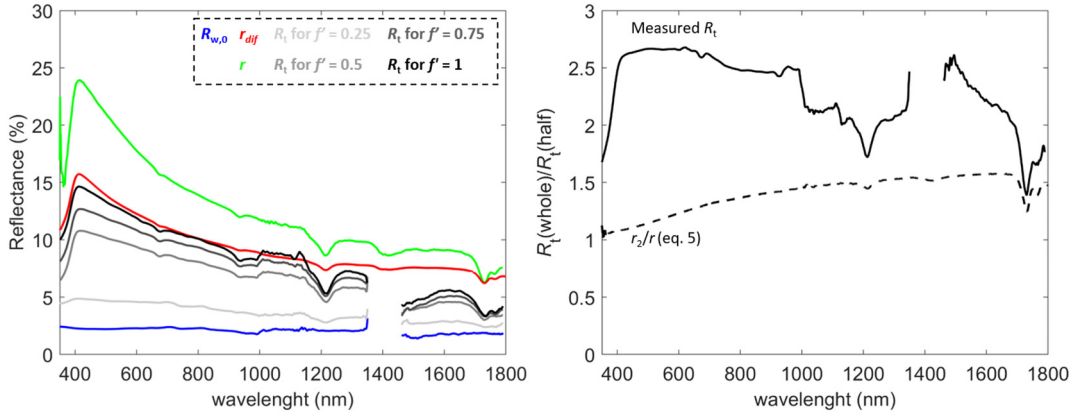

Fig. 7. (a) Line plots of R_t using HDPE milk bottles that were halved overlength (Fig. 1d), floating in the pond for a range of surface fractions $f' = \{0.25, 0.5, 0.75, 1\}$ indicated in shades of grey; $R_{w,0}$, r and r_{dif} are plotted in blue, green and red, respectively, and (b) ratios of reflectance of whole and of half milk bottles for $f' = 1$, with continuos line indicating measurements in the pond, and dashed line estimations for two layers in air, using laboratory measurements of r and Eq. (5). (For interpretation of the references to colour in this figure legend, the reader is referred to the web version of this article.)

(Fig. 5h). This implied that large bottles were more efficient light reflectors than small bottles, as possibly smaller gaps between smaller bottles were not big enough to explain the difference.

R_t for $f' = 1$ was higher than r but well below r_2 and calculated to vary between 16% and 17% either side of the PET absorption bandit 1660 nm (Eq. (5)). Hence, R_t was between r and r_2 as predicted for light passing through two layers of a transparent medium. Using large bottles, r (r_{dif}) was closest to R_t for f' of 0.75 (0.5). The ratio of R_t for large bottles and R_t for small bottles generally increased with increasing wavelength from 1.2 to about 1.7 until the water absorption band with a pronounced dip around 1130 nm (Fig. 8b). Beyond the water absorption band, the ratio varied between 1.4 and 1.6 with a dip around 1660 nm PET absorption band.

3.3. The concept model performance

The hyperspectral remote sensing model of Goddijn-Murphy et al. (2018) was tested using Eq. (1) with $\varepsilon = 1$ (neglecting the shading factor). The model should work for any wavelength in the VIS-NIR-SWIR and following Goddijn-Murphy et al. (2018) we used 850 nm. This wavelength was chosen as an optimum for low water- and high plastic reflectance outside the visible light spectrum so that plastic colour would not interfere. Scatter plots of $R_t(850)$ as a function of f', corresponding with the spectra shown in Fig. 5, are shown in Fig. 9. The (f', R_t) data were fitted to Eq. (1), with $R_{w,0}(850)$ the average over open water data and the plastic reflectance on water, $\rho_p(850)$, the fitting coefficient. Fig. 10 is similar, comparing whole double-layer, and half single-layer HDPE bottles, and small and large PET bottles. The regression results and their estimated errors are tabulated in Table 3. The regressions were highly significant for all plastic items, therefore supporting our model. $R_{w,0}(850)$ differed significantly between the three surveys and also changed during a survey. We believed the latter to be a consequence of fluctuating lighting conditions (such as passing clouds) and water surface roughness (generated by variable surface wind) and not of changing water composition. For each survey and for all surveys combined, $\rho_p(850)$ was significantly different between the plastic objects we used, an exception was halved HDPE milk bottles and PET bottles (small and large).

The last column in Table 3 contains information about the sensitivity of the single-band algorithm. Values of $dR_t(850)/df$ are used to indicate the sensitivity of the signal to changes in f', calculated as $\rho_p(850) - R_{w,0}(850)$ (Eq. (1)). The values were higher than previously predicted (Goddijn-Murphy et al., 2018), taking into account the different definitions of R_t. Goddijn-Murphy et al. (2018) base their prediction on Fresnel reflectance of skylight, which represents only part of the total reflectance of skylight and solar light. We found in this follow-up study that diffuse reflectance, r_{dif}, is a major contributor to r (Fig. 4) and reflects light in all directions so that the solar beam also reflects in nadir view. dR_t/df was closer to r_{dif} than to rF as presumed by Goddijn-Murphy et al. (2018). We investigated the relation between r and r_{dif} to ρ_p further.

Coefficients of reflectance measured in the laboratory, $r(850)$ and

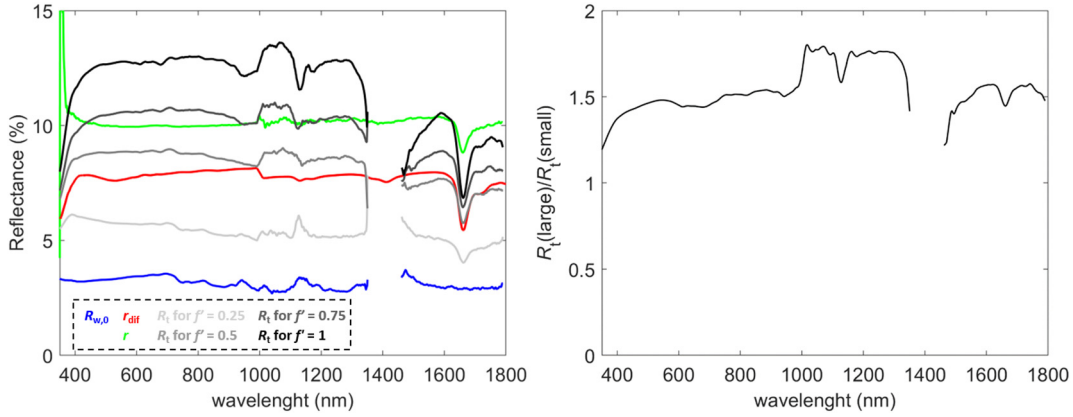

Fig. 8. (a) Line plots of R_t of large PET soft drink bottles (Fig. 1e), floating in the pond for a range of surface fractions $f' = \{0.25, 0.5, 0.75,1\}$ indicated in shades of grey; $R_{w,0}$, r and r_{dif} are plotted in blue, green and red, respectively, and (b) ratios of reflectance of large and of small PET bottles for $f' = 1$. (For interpretation of the references to colour in this figure legend, the reader is referred to the web version of this article.)

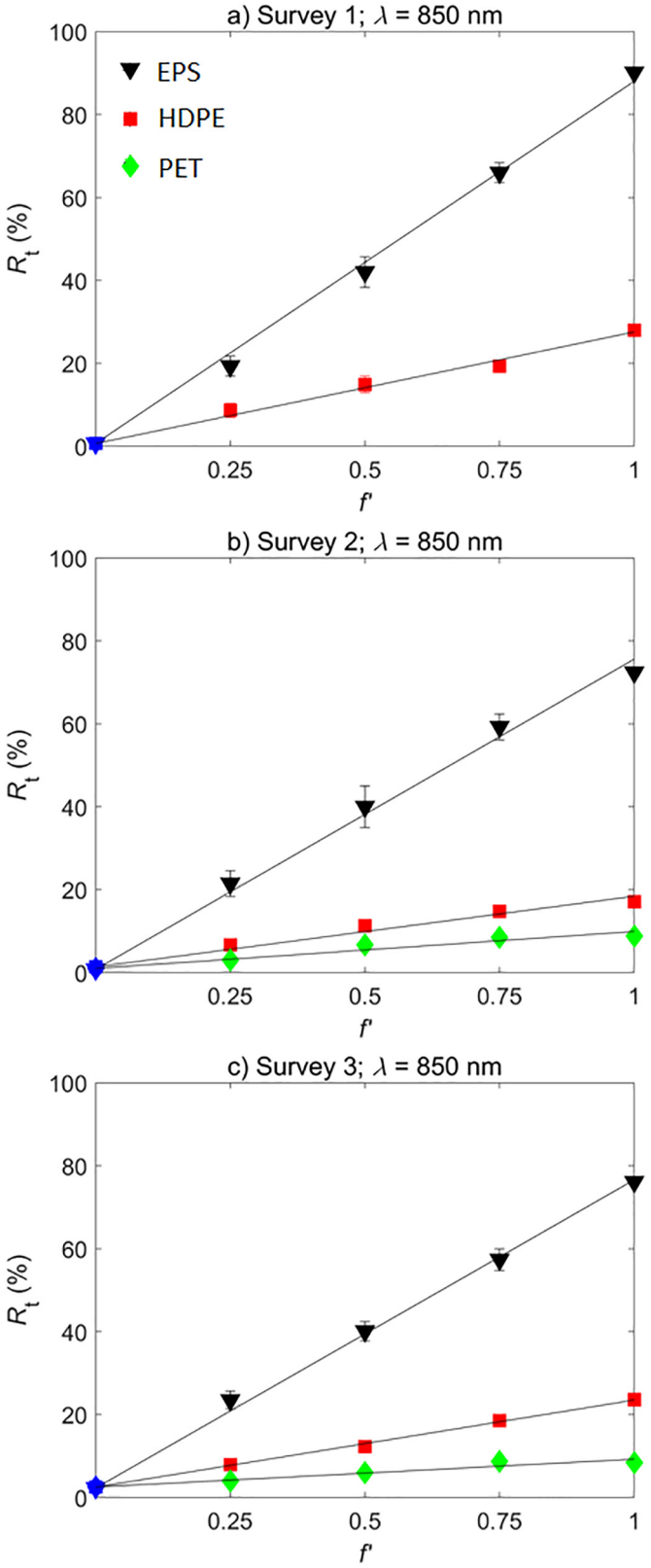

Fig. 9. Scatter plots of $R_t = R_t(850)$ as a function of f' for (a) survey1, (b) survey 2, and (c) survey 3. $R_{w,o}(850)$ is plotted in blue, and R_t of EPS, HDPE and PET as black triangles, red squares and green diamonds, respectively; the error bars indicate the standard errors of the mean over the four repeat measurements and the lines the fits of (f', $R_t(850)$) to Eq. (1) using $\varepsilon = 1$ (Table 3). (For interpretation of the references to colour in this figure legend, the reader is referred to the web version of this article.)

$r_{dif}(850)$, of one layer, and $r_2(850)$ and $r_{dif2}(850)$ derived for two layers are summarized in Table 4. For EPS, $\rho_p(850)$ agreed well with $r(850)$ for survey 1 but was smaller than $r(850)$ for the following surveys. For the one layer of a halved HDPE bottle, $r(850)$ was greater than $\rho_p(850)$ although the significance of the difference was marginal. For whole HDPE milk bottles, $\rho_p(850)$ matched $r_2(850)$ during survey 2 but during the other surveys $\rho_p(850)$ was considerably higher. Like for EPS, $\rho_p(850)$ was largest for survey 1. For small PET bottles, $\rho_p(850)$ was similar to $r(850)$ while for large PET bottles $\rho_p(850)$ was higher and between $r(850)$ and $r_2(850)$ as predicted. In summary, we could not satisfactorily calculate field measurements of ρ_p from reflectance coefficients r or r_2 for all plastic items. We believe these measurements should be repeated under more constant lighting conditions.

The influence of litter height on $R_t(\lambda)$ was clearly visible for EPS (Fig. 6). Corresponding $\rho_p(\lambda)$ appeared to saturate with height, and the saturation curve was dependent on wavelength (Fig. 11). For 850 nm, $\rho_p(850)$ levelled off at $-0.8\,cm^{-1}$ exponential rate to 25% while at the EPS absorption peak $\rho_p(1680)$ the respective values were $-0.4\,cm^{-1}$ and 18%.

3.3.1. Shading factor

The shading factor $\varepsilon(f,\lambda)$ in Eq. (1) is an effort to account for the reduction of subsurface light introduced by the presence of plastic and defined by the subsurface ratio of downwelling radiance in the presence of surface plastic and without. Goddijn-Murphy et al. (2018) derived an approximation $(1 - c_1 f) / (1 - c_2 f) \approx (1 - c_1 f)$ for ε. The denominator can be approximated by one because c_2 equals the product of subsurface plastic reflectance, ρ_{pw}, and subsurface water reflectance, r_{ws}, so that $\rho_{pw} r_{ws} f \approx 0$. The term c_1 is described by $(1 - \tau_{pw}/\tau_w)$, with τ_{pw} and τ_w the transmission coefficient of down welling radiance through the floating plastic and through the open water surface respectively. Regressing our measurement data against $R_t = (1 - c_1 f) R_{w,o} + f'(\rho_p - (1 - c_1 f) R_{w,0})$ instead of using $\varepsilon = 1$ in Eq. (1) did indeed somewhat improve the regressions for those with a coefficient of determination (R^2) smaller than 0.92 (Table 3). We found values for c_1 ranging from -6 ± 1 (HDPE, survey 2; $R^2 = 1.00$) to -1 ± 5 (small PET, survey 3; $R^2 = 0.89$), which would imply $\tau_{pw} > \tau_w$ and hence an intensification of subsurface light instead of the expected darkening introduced by plastic at the water surface. We could therefore not show evidence for a shading effect.

3.3.2. Dual band algorithm

We assessed the dual band theory (Eq. (2)) by linear regressing $\Delta R_t = R_t(\lambda_1) - R_t(\lambda_2)$ against f' (forced through zero), so that the regression coefficient signified $\Delta\rho_p = \rho_p(\lambda_1) - \rho_p(\lambda_2)$. Regression results are shown in Table 5. For λ_1 we chose 850 nm where ρ_p is high and outside VIS, and λ_2 where ρ_p is low (plastic absorption band) and where $R_{w,0}(\lambda_2) \approx R_{w,0}(\lambda_1)$. Light reflected at water at wavelengths larger than 850 nm consists of direct reflected light, which is practically wavelength independent, and hence we chose $\lambda_2 > \lambda_1$ in the SWIR. We found plastic absorption bands at 1680 nm, 1730 nm and 1660 nm for EPS, HDPE, and PET respectively (Fig. 4). We applied the dual band algorithm for the three plastic types also at the PET absorption band to evaluate how one common value of λ_2 performs. If we regard $d\Delta R_t / df' = \Delta\rho_p$ as a rate of sensitivity of the RS signal to changes in f', we can see it is strongest for EPS and weakest for PET with HDPE in the middle, similar to the single band signal. Naturally, for each plastic $\Delta\rho_p$ is highest if λ_2 is selected at its specific absorption peak. However, using λ_2 at the PET absorption peak, $\Delta\rho_p$ for EPS and HDPE is higher than for PET itself. The signal of the dual-band signal is generally weaker than of the single-band (dR_t/df in Table 3), but for HDPE not in a major way if λ_2 is chosen at the HDPE absorption peak.

For comparing field data with laboratory results we calculated delta_r_{dif} and delta_r for one layer, and delta_r_{dif2} and delta_r_2 for two layers, of plastic (Table 6). For EPS, with $\lambda_1 = 850$ nm and λ_2 at its absorption band at 1680 nm, Δr_{dif} and Δr agreed with $\Delta\rho_p$ during

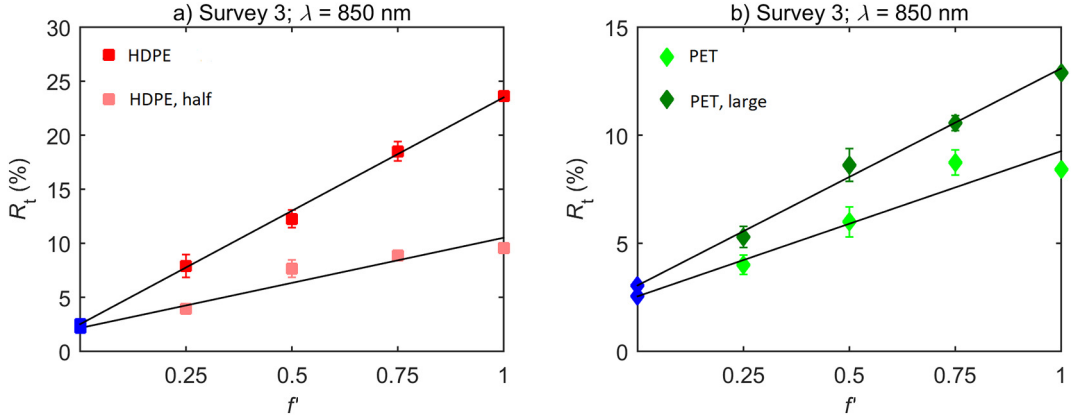

Fig. 10. Scatter plots of $R_t = R_t(850)$ as a function of f', with the error bars indicating the standard errors of the mean over the four repeat measurements and the lines the fits of (f', R_t) to Eq. (1) using $\varepsilon = 1$ (Table 3). $R_{w,0}(850)$ is plotted as blue dots, and (a) R_t using HDPE whole/half milk bottles as red/pink squares, and (b) R_t using PET small/large bottles as light/dark green diamonds. (For interpretation of the references to colour in this figure legend, the reader is referred to the web version of this article.)

Table 3
Regression results of a fit of (f', $R_t(850)$) to Eq. (1) using $\varepsilon = 1$, with $R_{w,0}$ mean $R_{w0}(850)$ and ρ_p the fit coefficient; $\delta R_{w,0}$ is the standard error of the mean, $\delta\rho_p$ the error of the fit coefficient with 95% confidence bounds, R^2 the 'coefficient of determination', and dR_t/df' estimated by ρ_p-$R_{w,0}$.

Object	Survey	$R_{w,0}$ (%)	$\delta R_{w,0}$ (%)	ρ_p (%)	$\delta\rho_p$ (%)	R^2	dR_t/df' (%)
EPS	1	0.713	0.004	88	5	1.00	87
	2	0.78	0.04	76	6	0.98	75
	3	2.28	0.04	77	4	0.99	75
	1, 2 and 3	*1.3*	*0.5*	*80*	*4*	*0.96*	*79*
HDPE	1	0.67	0.05	28	3	0.98	27
	2	1.38	0.05	18	3	0.91	17
	3	2.51	0.01	24	1	1.00	21
	1, 2 and 3	*1.5*	*0.5*	*23*	*2*	*0.82*	*22*
HDPE_h	3	2.16	0.04	11	2	0.85	9
PET	2	1.02	0.03	10	1	0.92	9
	3	2.54	0.01	9	2	0.86	6
	2 and 3	*1.5*	*0.8*	*9.5*	*1*	*0.85*	*8*
PET_L	3	3.05	0.05	13	1	0.99	10

Table 4
Coefficients of total and diffuse reflectance, r and r_{dif}, of one layer in air measured in the laboratory and calculated for two layers (Fig. 3), respectively r_2 and r_{dif2}, using t, r and r_{dif} (Eq. (5)).

Polymer	$r(850)$ (%)	$r_2(850)$ (%)	$r_{dif}(850)$ (%)	$r_{dif2}(850)$ (%)
EPS	90.1	NA	90.3	NA
HDPE	13.3	18.5	9.7	13.5
PET	10.0	16.8	8.0	13.5

surveys 1 and 2 but both significantly underestimated $\Delta\rho_p$ during survey 3. Using λ_2 at 1660 nm, Δr_{dif} and Δr underestimated $\Delta\rho_p$ during all surveys. For single-layered half HDPE bottles, Δr agreed with $\Delta\rho_p$ using both λ_2 wavelengths 1730 and 1660 nm. For bottles we should use r_2 (Eq. (5)), instead of r, to calculate Δr_2 and predict $\Delta\rho_p$. This improved the estimations for PET bottles using Δr_2 (Δr_{dif2}) for small (large) bottles. For whole HDPE bottles, Δr_{dif2} and Δr_2 underestimated $\Delta\rho_p$ with λ_2 at its absorption band and even more at 1660 nm. In summary, for single layers $\Delta\rho_p$ is well predicted by Δr if λ_2 is at the polymer specific absorption band while for double layers the relation is more complicated.

4. Discussion

The lighting conditions during our surveys were not as usual for RS

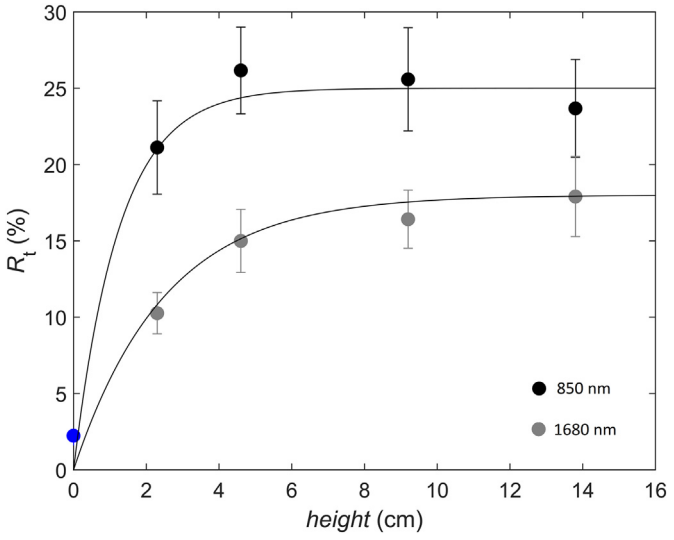

Fig. 11. Scatter plots of $R_t(\lambda)$ as a function of EPS height h [cm] using f' of 0.25; black/grey dots indicate $\lambda = 850/1680$ nm and black/grey lines respective curve fits $R_t(850) = 25(1 - \exp(-0.8\,h))$ and $R_t(1680) = 18(1 - \exp(-0.4\,h))0$.

Table 5
Linear regression results of $R_t(\lambda_1) - R_t(\lambda_2)$ against f' (Eq. (2)) revealing fit coefficient $\Delta\rho_p(\lambda_1,\lambda_2)$ with $\lambda_1 = 850$ nm and λ_2 as indicated; $\delta\Delta\rho_p$ is the error of the fit with 95% confidence bounds, and R^2 the 'coefficient of determination'.

Object	Survey	$\Delta\rho_p$	$\delta\Delta\rho_p$	R^2	$\Delta\rho_p$	$\delta\Delta\rho_p$	R^2
		λ_2 = 1680 nm			λ_2 = 1660 nm		
EPS	1	25	2	0.99	13	1	0.99
	2	23	2	0.98	14	1	0.99
	3	37	4	0.99	30	5	0.97
	1, 2 and 3	*28*	*4*	*0.80*	*19*	*5*	*0.54*
		λ_2 = 1730 nm			λ_2 = 1660 nm		
HDPE	1	25	2	0.99	16	1	1.00
	2	15	2	0.96	11	1	0.99
	3	19	1	0.99	12	1	1.00
	1, 2 and 3	*20*	*3*	*0.80*	*13*	*2*	*0.83*
HDPE_h	3	7	2	0.87	5	1	0.83
		λ_2 = 1660 nm					
PET	2	5	1	0.93			
	3	4	1	0.83			
	2 and 3	*4.6*	*0.6*	*0.83*			
PET_L	3	6.1	0.7	0.98			

Table 6
Calculations of $\Delta r = r(850) - r(\lambda_2)$ and $\Delta r_2 = r_2(850) - r_2(\lambda_2)$ using Eqs. (3) & (5) with total and diffuse reflectance, and λ_2 as indicated.

Object	λ_2	Δr_{dif} (%)	Δr_{dif2} (%)	Δr (%)	Δr_2 (%)
EPS	1680	25	NA	23	NA
	1660	10	NA	9.4	NA
HDPE	1730	3.7	5.9	7.3	11
	1660	2.3	1.9	4.3	4.3
PET	1660	2.8	5.9	1.3	4.1

missions which are routinely executed during high solar angles and clear skies. However, we could use our measurements to study the interaction of sunlight with a plastic littered water surface. The fitting coefficients of our optical model were expected to change with lowering solar angle and increasing fraction diffuse skylight but not to necessarily perform worse. This would depend on how different the reflecting properties of the plastic litter are from the water it is floating on. Nevertheless, the light levels were low and the noise of the spectroradiometer increased with decreasing light levels and increasing wavelength. We were able to obtain reflectance spectra and verify our hyperspectral concept model for wavelengths smaller 1790 nm. Plastic reflectance in the field was loosely related to the reflectance coefficient of the plastic measured in the laboratory, but the changeable lighting conditions between surveys and during surveys made it difficult to be precise.

The plastic items we measured were a selection of all buoyant plastics littering the ocean, chosen to cover a range of optical properties and because of their convenience. They were (1) white, opaque EPS building foam, (2) white semi-transparent HDPE milk bottles, and (3) clear transparent PET soft drink bottles. They were useful to verify the concept of our optical model and easy to handle, but we necessarily excluded other types of important plastic litter items such as fishing nets, ropes, plastic sheets, buoys and fish boxes, and items made of different compositions, for example, polypropylene (PP) and polyvinyl chlorine (PVC). We also have to keep in mind that plastic items are not the only buoyant litter that reflect light and that we should consider debris such as drift wood and steel drums. However, this might be less of an issue in the open ocean. Comparing mean litter densities from recent worldwide data, Galgani et al. (2015) found that over 70%, and frequently close to a 100%, consists of plastic. In the GPGP, plastics represent > 99.9% of marine litter (Lebreton et al., 2018). We could develop RS algorithms based on more than one or two wavelengths to separate between different polymers (Garaba and Dierssen, 2018) and plastic from non-plastic litter. We could also apply shape recognition techniques to visual images to obtain more information about the litter (Martin et al., 2018). It is likely that successful RS algorithms for marine plastic will be based on complimentary approaches.

The chemical composition of the plastics explained their spectral signatures and the location of their absorption bands determined by their absorption spectra (Fig. 4). The location of these absorption bands is of major importance when developing RS algorithms but our aim was not to add to the spectral reference library of plastics (e.g., Garaba and Dierssen, 2017, 2018). Instead, we focussed on other, physical, plastic litter properties that obviously affect light reflectance. We could illustrate the importance of this by shattering a clear glass bottle into very small pieces. A pile of accumulated glass fragments will no longer be see-through and therefore reflect light differently than the glass bottle, although it is composed of the same material. In this study, we look at the 'glass bottle'. We used 850 nm wavelength for our evaluation, at this NIR wavelength, plastic reflectance was high and water reflectance low, but our optical model (Eq. (1)) could apply to any wavelength such as at an absorption band. Another reason for choosing 850 nm is that it could benefit the use of cameras with a NIR-band for monitoring drifting plastic.

Our measurements implied that reflectance increased with increasing opacity, item height, volume and number of layers. As the plastic littering the oceans is a mix of all kinds of items, one universal RS algorithm applicable to marine plastic litter is therefore not feasible. But even if we could, how do we express the unit of plastic concentration? Is percentage surface coverage, like we used in this paper, adequate? Or should it be a numerical concentration defined by number of particles per unit surface (classified by size), or a mass concentration? Particle numbers are used in the assessment of exposure risks while measurements of mass are required for mass balance and emission studies (van Sebille et al., 2015). As a first approach we could quantify surface plastic concentration in terms of the reflectance of one type of plastic, for example a sheet of white EPS and normalize R_t to ρ_p of EPS and call the unit [reps], i.e., $R_{tn} = R_t/\rho_{p,EPS}$ [reps]. We could then combine R_{tn} with knowledge of marine plastic litter constituents, such as collected by Eriksen et al. (2014) and Lebreton et al. (2018), and plastic item specific ρ_p values to derive total numerical/mass surface concentration. For developing practical RS algorithms, we need to acquire knowledge about what floating plastic litter is composed of. Another approach could be to define a threshold for plastic detection and classify pixels as plastic present or no plastic present (regardless of plastic concentration in ground pixel).

By finding macroplastics, we anticipate to find a growing source of microplastics (Filella, 2015) and we could use the anticipated correlation between the two to estimate the abundance of microplastics. The relation between micro- and macroplastics needs further study; at the moment not near as much microplastic has been found as we would expect (e.g., Eriksen et al., 2014). One of the removal processes is the sinking of microplastics (enhanced by biofouling), making them 'invisible' to infrared light. The absorption coefficient of pure water, a_w, is $0.041/5.0\ cm^{-1}$ at λ of 850/1660 nm (Irvine and Pollack, 1968), which means that 90% (99%) of light just below the water surface is absorbed by water over the top 0.5 m/0.5 cm (1 m/1 cm) (estimated by, % absorbed = $100 \times e^{-ad}$ for path length d). Studies of depth profiles of marine plastic litter could help calculate subsurface plastic from surface observations (Kooi et al., 2016).

Garaba and Dierssen (2018) show that the reflectance of marine-harvested microplastics is significantly suppressed by wetting with filtered seawater, from 12% in the UV to nearly 90% in the SWIR. This cannot be explained by just light absorption in a thin film of water, for example at 600 nm they measure a reduction of about 75% (Fig. 6 in Garaba and Dierssen, 2018). At this wavelength a_w is $0.0015\ cm^{-1}$ (Irvine and Pollack, 1968) independent of salinity (Pegau et al., 1997) and a 75% reduction would require almost 2 m of water. Other mechanisms contribute to the weakening of reflectance at a wet surface (Lekner and Dorf, 1988). For finely divided media, such as sand and aggregated microplastics, the idea of enhanced forward scattering when the interstitial space in the medium is filled with water would seem to apply (Lekner and Dorf, 1988). For solid rough surfaces (such as of macrolitter), reduced reflectance by a thin film of water is better explained by water having a higher refractive index than air, which can cause a fraction of diffuse reflected light at the plastic to totally reflect back down at the water-air interface (Lekner and Dorf, 1988). The rougher the surface, the more diffuse reflection, and thus the more total internal reflection at the water-air interface. (A ray of light reflecting at an optically smooth surface will not be totally reflected at a water-air interface on top.) As the EPS foam consists of small EPS beads pressed together it could be an intermediate case so that enhanced forward scattering also contributed. Compared to absorption coefficient, the refractive index of water does not change much with wavelength. Water absorption largely increases with increasing wavelength and becomes more important in the SWIR spectrum, enhancing the suppression of reflectance in the NIR and SWIR. We did not control the wetness of the plastic items in our field experiment, we considered them to be a random mix of dry and wet, but it should be studied in follow-up research. Another subject of further research should be the effect of biofouling and weathering of the litter on its optical properties.

Using the hyperspectral model, we explored options for a simple working RS method. The single-band is expected to be more sensitive than the dual-band signal but for the single-band, reflectance of clear water, $R_{w,0}$, needs to be known a priori. If $R_{w,0}$ cannot be estimated from measurements, models, historic data, or otherwise, but is not expected to change much, the single-band signal can still give us relative values, i.e. spatial distribution patterns or trends in abundance. An advantage of the single-band algorithm is that it needs only one band in the NIR, and that the selection of wavelength centre and width does not need to be as precise as for the dual-band algorithm. Now that low-cost digital cameras that feature a band in the NIR are coming on to the market, this could make RS affordable. We do not need to know $R_{w,0}$ in the dual-band algorithm but its signal is less sensitive to changes in surface plastic. Also, the wavelength centre and width of the second band in the SWIR are critical as it should contain a plastic absorption band. Our experiments were executed using plastic floating in an inland water. The results should be transferable to other water types such as coastal and oceanic, as long as its reflectance is significantly lower than that of plastic. It is difficult to determine what the smallest surface concentration of detectable plastic litter within a ground FOV could be as it greatly depends on the reflective properties of the plastic (ρ_p or $\Delta\rho_p$), how certainly we know $R_{w,0}$, and the noise in measurements of R_t. This should be a subject of further experiments under better lighting conditions.

5. Conclusion

A handheld spectroradiometer can easily observe plastic litter floating on a water surface and our observations confirmed a theoretical concept model (Goddijn-Murphy et al., 2018). Reflectance of the plastic items floating on the water surface in natural daylight loosely corresponded with the reflectance coefficients of the materials obtained in the laboratory. We believe that the varying lighting environment between and during the surveys affected this correspondence. The relation between measured reflectance and plastic surface fraction was highly sensitive to the type of polymer and also to the transparency, shape and surface roughness of the plastic item. We can therefore not propose one general RS algorithm for estimating surface fraction of plastic litter floating on natural waters, let alone weight or numerical concentration, from light reflectance data alone. Studies about the constitution of marine plastic litter (e.g., types and sizes, and relation between macro and micro) would help advance our RS algorithms. We derived plastic item specific RS algorithms for low solar elevation angles and in varying presence of clouds, and we expect RS parameters to be different and more consistent under clear skies and high solar elevation angles.

Acknowledgements

This work was supported by the Carnegie Trust for the Universities of Scotland [Research Incentive Grant: 70649]. The authors acknowledge and are grateful for the training and loan of a spectroradiometer by the NERC Field Spectroscopy Facility.

References

ASD Inc, 2008. Integrating sphere user manual. ASD. Document 600660 Rev. A. www.Asdi.com.

Asner, 2016. Workshop on mission concepts for marine debris sensing, January 19–21, 2016, east-west center of the University of Hawaii at Manoa, Honolulu, Hawaii. Available online. http://iprc.soest.hawaii.edu/NASA_WS_MD2016/pdf/Asner2016.pdf, Accessed date: 6 February 2018.

Batchelli, S., Muller, F.L.L., Chang, K.-C., Lee, C.-L., 2010. Evidence for strong but dynamic iron-humic colloidal associations in humic-rich coastal waters. Environ. Sci. Technol. 44 (22), 8485–8490. https://doi.org/10.1021/es101081c.

Bowers, D.G., Harker, G.E.L., Smith, P.S.D., Tett, P., 2000. Optical properties of a region of freshwater influence (the Clyde Sea). Estuar. Coast. Shelf Sci. 50, 717–726. https://doi.org/10.1006/ecss.1999.0600.

Cózar, A., Echevarríaa, F., González-Gordillo, J.I., Irigoien, X., Úbeda, B., Hernández-León, S., Palma, A.T., Navarro, S., García-de-Lomas, J., Ruiz, A., Fernández-de-Puelles, M.L., Duarte, C.M., 2014. Plastic debris in the open ocean. PNAS 111 (28), 10239–10244. https://doi.org/10.1073/pnas.1314705111.

Cózar, A., Martí, E., Duarte, C.M., García-de-Lomas, J., van Sebille, E., Ballatore, T.J., Eguíluz, V.M., González-Gordillo, J.I., Pedrotti, M.L., Echevarría, F., Troublè, R., Xabier Irigoien, X., 2017. The Arctic Ocean as a dead end for floating plastics in the North Atlantic branch of the thermohaline circulation. Sci. Adv. 3, e1600582. https://doi.org/10.1126/sciadv.1600582.

Driedger, A.G.J., Dürr, H.H., Mitchell, K., Van Cappellen, P., 2015. Plastic debris in the Laurentian Great Lakes: a review. J. Great Lakes Res. 41 (1), 9–19. https://doi.org/10.1016/j.jglr.2014.12.020.

Eriksen, M., Lebreton, L.C.M., Carson, H.S., Thiel, M., Moore, C.J., Borerro, J.C., Galgani, F., Ryan, P.G., Reisser, J., 2014. Plastic pollution in the world's oceans: more than 5 trillion plastic pieces weighing over 250,000 tons afloat at sea. PLoS One 9 (12), e111913. https://doi.org/10.1371/journal.pone.0111913.

Filella, M., 2015. Questions of size and numbers in environmental research on microplastics: methodological and conceptual aspects. Environ. Chem. 12 (5), 527–538. https://doi.org/10.1071/EN15012.

Galgani, F., Hanke, G., Maes, T., 2015. Global distribution, composition and abundance of marine litter. In: Bergmann, M., Gutow, L., Klages, M. (Eds.), Marine Anthropogenic Litter. Springer, Cham. https://doi.org/10.1007/978-3-319-16510-3_2.

Garaba, S.P., Dierssen, H.M., 2017. Spectral Reference Library of 11 Types of Virgin Plastic Pellets Common in Marine Plastic Debris. Data set available on-line. http://ecosis.orgEcological Spectral Information System (EcoSIS)https://doi.org/10.21232/C27H34.

Garaba, S.P., Dierssen, H.M., 2018. An airborne remote sensing case study of synthetic hydrocarbon detection using short wave infrared absorption features identified from marine-harvested macro- and microplastics. Remote Sens. Environ. 205, 224–235. https://doi.org/10.1016/j.rse.2017.11.023.

Goddijn-Murphy, L., Peters, S., Van Sebille, E., James, N.A., Gibb, S., 2018. Concept for a hyperspectral remote sensing algorithm for floating marine macro plastics. Mar. Pollut. Bull. 126, 255–262. https://doi.org/10.1016/j.marpolbul.2017.11.011.

Gordon, H.R., Brown, O.B., Jacobs, M.M., 1975. Computed relationships between the inherent and apparent optical properties of a flat homogeneous ocean. Appl. Opt. 14, 417–427.

Hecht, E., Zajac, A., 1974. Optics. Addison-Wesley Publishing Company, Inc., Massachusetts.

Hoffman, M.J., Hittinger, E., 2017. Inventory and transport of plastic debris in the Laurentian Great Lakes. Mar. Pollut. Bull. 115, 273–281. https://doi.org/10.1016/j.marpolbul.2016.11.061.

Irvine, W.M.J.B., Pollack, J.B., 1968. Infrared optical properties of water and ice spheres. Icarus 8.

Jambeck, J.R., Geyer, R., Wilcox, C., Siegler, T.R., Perryman, M., Andrady, A., et al., 2015. Plastic waste inputs from land into the ocean. Science 347 (6223), 768–771. https://doi.org/10.1126/science.1260352.

Jerlov, N.G., 1968. Optical Oceanography. Elsevier Publishing Company, Amsterdam.

Kooi, M., Reisser, J., Slat, B., Ferrari, F.F., Schmid, M.S., Cunsolo, S., Brambini, R., Noble, K., Sirks, L.-A., Linders, T.E.W., Schoeneich-Argent, R.I., Koelmans, A.A., 2016. The effect of particle properties on the depth profile of buoyant plastics in the ocean. Sci. Rep. 6, 33882. https://doi.org/10.1038/srep33882.

Kukulka, T., Proskurowski, G., Morét-Ferguson, S., Meyer, D.W., Law, K.L., 2012. The effect of wind mixing on the vertical distribution of buoyant plastic debris. Geophys. Res. Lett. 39 (L07601). https://doi.org/10.1029/2012GL051116.

Law, K.L., Morét-Ferguson, S., Maximenko, N.A., Proskurowski, G., Peacock, E.E., Hafner, J., Reddy, C.M., 2010. Plastic accumulation in the North Atlantic subtropical gyre. Science 329, 1185–1188. https://doi.org/10.1126/science.1192321.

Law, K.L., Morét-Ferguson, S.E., Goodwin, D.S., Zettler, E.R., DeForce, E., Kukulka, T., Proskurowski, G., 2014. Distribution of surface plastic debris in the eastern Pacific Ocean from an 11-year data set. Environ. Sci. Technol. 48, 4732–4738. https://doi.org/10.1021/es4053076.

Lebreton, L.C.-M., Greer, S.D., Borerro, J.C., 2012. Numerical modelling of floating debris in the world's oceans. Mar. Pollut. Bull. 64 (3), 653–661. https://doi.org/10.1016/j.marpolbul.2011.10.027.

Lebreton, L., Slat, B., Ferrari, F., Sainte-Rose, B., Aitken, J., Marthouse, R., Hajbane, S., Cunsolo, S., Schwarz, A., Levivier, A., Noble, K., Debeljak, P., Maral, H., Schoeneich-Argent, R., Brambini, R., Reisser, J., 2018. Evidence that the Great Pacific Garbage Patch is rapidly accumulating plastic. Sci. Rep. 8 (4666). https://doi.org/10.1038/s41598-018-22939-w.

Lekner, J., Dorf, M.C., 1988. Why some things are darker when wet. Appl. Opt. 27 (7), 1278–1280. https://doi.org/10.1364/AO.27.001278.

Mac Arthur, A.A., MacLellan, C., Malthus, T.J., 2012. The fields of view and directional response functions of two field spectroradiometers. IEEE Trans. Geosci. Remote Sens. 50 (10), 3892–3907. https://doi.org/10.1109/TGRS.2012.2185055.

Martin, C., Parkes, S., Zhang, Q., Zhangc, X., McCabe, M.F., Duarte, C.M., 2018. Use of unmanned aerial vehicles for efficient beach litter monitoring. Mar. Pollut. Bull. 131, 662–673. https://doi.org/10.1016/j.marpolbul.2018.04.045.

Maximenko, N.A., Hafner, J., Niiler, P.P., 2012. Pathways of marine debris derived from trajectories of Lagrangian drifters. Mar. Pollut. Bull. 65 (1–3), 51–62. https://doi.org/10.1016/j.marpolbul.2011.04.016.

Maximenko, N., Arvesen, J., Asner, G., Carlton, J., Castrence, M., Centurioni, L., et al., 2016. Remote sensing of marine debris to study dynamics, balances and trends. In: Community White Paper Produced at the Workshop on Mission Concepts for Marine Debris Sensing, January 19–21, 2016, East-West Center of the University of Hawaii at Manoa, Honolulu, Hawaii, (Submitted to: Decadal Survey for Earth Science and Applications from Space).

Morel, Y.A., Prieur, L., 1977. Analysis of variations in ocean color. Limnol. Oceanogr. 22 (4), 709–722.

Pegau, S.W., Gray, D., Zaneveld, R.J., 1997. Absorption and attenuation of visible and near-infrared light in water: dependence on temperature and salinity. Appl. Opt. 36 (24), 6035–6046. https://doi.org/10.1364/AO.36.006035.

Ryan, P.G., 2015. Does size and buoyancy affect the long-distance transport of floating debris? Environ. Res. Lett. 10, 084019. https://doi.org/10.1088/1748-9326/10/8/084019.

Schmidt, C., Krauth, T., Wagner, S., 2017. Export of plastic debris by rivers into the sea. Environ. Sci. Technol. 51 (12246–12253), 51. https://doi.org/10.1021/acs.est.7b02368.

Scientific Polymer, Inc, 2013. Reefractive Index of Polymers. Technical Library. http://scientificpolymer.com/technical-library/refractive-index-of-polymers-by-index/, Accessed date: 20 December 2017.

Stramski, D., Woźniak, S., 2005. On the role of colloidal particles in light scattering in the ocean. Limnol. Oceanogr. 50 (5), 1581–1591. https://doi.org/10.4319/lo.2005.50.5.1581.

van Sebille, E., England, M.H., Froyland, G., 2012. Origin, dynamics and evolution of ocean garbage patches from observed surface drifters. Environ. Res. Lett. 7, 044040. https://doi.org/10.1088/1748-9326/7/4/044040.

van Sebille, E., Wilcox, C., Lebreton, L., Maximenko, N.A., Hardesty, B.D., van Franeker, J.A., et al., 2015. A global inventory of small floating plastic debris. Environ. Res. Lett. 10 (12), 124006. https://doi.org/10.1088/1748-9326/10/12/124006.

Veenstra, T.S., Churnside, J.H., 2012. Airborne sensors for detecting large marine debris at sea. Mar. Pollut. Bull. 65, 63–68. https://doi.org/10.1016/j.marpolbul.2010.11.018.